


Article

Measures to Reduce the N₂O Formation at Perovskite-Based Lean NO_x Trap Catalysts under Lean Conditions

Sabrina I. Ecker^{1,2,*}, Jürgen Dornseiffer¹, Stefan Baumann¹ , Olivier Guillon^{1,3}, Henny J. M. Bouwmeester^{1,4} and Wilhelm A. Meulenber^{1,2}

- ¹ Forschungszentrum Jülich GmbH, Institute of Energy and Climate Research, IEK-1: Materials Synthesis and Processing, 52425 Jülich, Germany; j.dornseiffer@fz-juelich.de (J.D.); s.baumann@fz-juelich.de (S.B.); o.guillon@fz-juelich.de (O.G.); h.j.m.bouwmeester@utwente.nl (H.J.M.B.); w.a.meulenber@fz-juelich.de (W.A.M.)
- ² Inorganic Membranes, Faculty of Science and Technology, University of Twente, P.O. Box 217, 7500 AE Enschede, The Netherlands
- ³ Jülich Aachen Research Alliance: JARA Energy, Forschungszentrum Jülich GmbH, 52425 Jülich, Germany
- ⁴ Electrochemistry Research Group, Faculty of Science and Technology, University of Twente, P.O. Box 217, 7500 AE Enschede, The Netherlands
- * Correspondence: s.ecker@fz-juelich.de; Tel.: +49-246104069466

Abstract: The net oxidising atmosphere of lean burn engines requires a special after-treatment catalyst for NO_x removal from the exhaust gas. Lean NO_x traps (LNT) are such kind of catalysts. To increase the efficiency of LNTs at low temperatures platinumised perovskite-based infiltration composites La_{0.5}Sr_{0.5}Fe_{1-x}M_xO_{3-δ}/Al₂O₃ with M = Nb, Ti, Zr have been developed. In general, platinum based LNT catalysts show an undesired, hazardous formation of N₂O in the lean operation mode due to a competing C₃H₆-selective catalytic reduction (SCR) at the platinum sites. To reduce N₂O emissions an additional Rh-coating, obtained by incipient wetness impregnation, besides the Pt coating and a two-layered oxidation catalyst (2 wt.% Pd/20 wt.% CeO₂/alumina)-LNT constitution, has been investigated. Though the combined Rh-Pt coating shows a slightly increased NO_x storage capacity (NSC) at temperatures above 300 °C, it does not decrease N₂O formation. The layered oxidation catalyst-LNT system shows a decrease in N₂O formation of up to 60% at 200 °C, increasing the maximum NSC up to 176 μmol/g. Furthermore, the NSC temperature range is broadened compared to that of the pure LNT catalyst, now covering a range of 250–300 °C.

Keywords: Lean NO_x trap (LNT); N₂O formation; C₃H₆-SCR (selective catalytic reduction); precious metal (Pt, Rh, Pd); layered catalyst constitution



Citation: Ecker, S.I.; Dornseiffer, J.; Baumann, S.; Guillon, O.; Bouwmeester, H.J.M.; Meulenber, W.A. Measures to Reduce the N₂O Formation at Perovskite-Based Lean NO_x Trap Catalysts under Lean Conditions. *Catalysts* **2021**, *11*, 917. <https://doi.org/10.3390/catal11080917>

Academic Editors: Filipa Ribeiro and Patrick Da Costa

Received: 28 June 2021

Accepted: 22 July 2021

Published: 29 July 2021

Publisher's Note: MDPI stays neutral with regard to jurisdictional claims in published maps and institutional affiliations.



Copyright: © 2021 by the authors. Licensee MDPI, Basel, Switzerland. This article is an open access article distributed under the terms and conditions of the Creative Commons Attribution (CC BY) license (<https://creativecommons.org/licenses/by/4.0/>).

1. Introduction

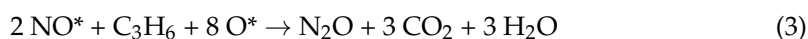
Lean-burn engines operating with air excess show high emissions of NO and NO₂, referred to as NO_x [1]. To reduce the emissions of these harmful gases additional after-treatment systems need to be included in the exhaust pathway [2]. Under ideal conditions [3,4] the selective catalytic reduction (SCR) catalyst [5,6] or the lean NO_x trap catalyst (LNT), also known as NO_x storage and reduction catalyst (NSR) [7], reduce NO_x selectively to N₂ and water. However, ideal conditions are rarely encountered due to the varying exhaust temperatures (150–500 °C) [8,9] giving rise to different exhaust gas compositions as a result of incomplete combustion processes [9,10] and side reactions [3,11–13]. Hence, side product formation of secondary pollutants N₂O and NH₃ occurs due to the use of catalytic after-treatment systems [14,15]. Whereas ammonia is able to reduce NO_x to N₂, N₂O is less reactive and still being emitted [16,17]. Nitrous oxide is proven to be one of the most dangerous greenhouse gases with a lifetime of 120–150 years and a global warming potential (GWP) which is almost 300 times higher than that of CO₂ [18]. Nonetheless, N₂O is rarely included in emission regulations. The United States Environmental Protection

Agency (U.S. EPA) has set N_2O emissions to a limit value of 0.010 g/mile for light-duty vehicles (2012–2016) [18]. In such vehicles, lean NO_x traps are the preferred after-treatment catalyst [19] as they are the most space-saving De NO_x systems.

LNTs, originally introduced as Pt-Ba/ Al_2O_3 , reduce NO_x by alternating lean-rich cycles of the engine. In a long-lasting lean operation phase (in excess of air), dominant NO is oxidised to NO_2 by platinum which is stored by sorption onto an (earth-) alkaline metal oxide in the form of nitrites and nitrates. After 60–120 s of storage, the engine operation mode changes to the short rich mode (in excess of fuel), whereby reductives, such as H_2 , CO and hydrocarbons (HC), are produced. These gases initiate the desorption of the stored nitrites and nitrates, reducing them to N_2 , N_2O and NH_3 [7].

As nitrous oxide formation is generally related to the regeneration of LNT catalysts, most studies deal with investigations towards N_2O evolution in the rich phase and/or during the switch from rich to lean conditions and vice versa [10,20–22]. However, a few studies have reported N_2O formation in the lean operation mode due to NO_x reduction on Pt-based LNT catalysts in the presence of reductives. Huang et al. [8] observed a decrease of 30% in the NO concentration over Pt/CaO/ Al_2O_3 in excess of oxygen due to reduction by CO and C_3H_6 . Similar behaviour has been observed for the Pt/ CeO_2 -Zr O_2 catalyst investigated by Masdrag et al. [23] showing formation of N_2O in the temperature range of 200–300 °C. The latter authors studied the impact of H_2 , CO and C_3H_6 by single and mixed feed gas experiments and identified a temperature-dependent influence on N_2O evolution. Whereas the order of reducibility at 200 °C was $\text{H}_2 > \text{CO} > \text{C}_3\text{H}_6$ (≈ 0), it was found to change by an increase in temperature to 300 °C to $\text{C}_3\text{H}_6 > \text{H}_2 > \text{CO}$ (≈ 0). The results of Masdrag et al. [23] and Huang et al. [8] are merely consistent with previous results on Platinum Group Metal (PGM)-based catalysts [24–26]. In 1991, Hamada et al. [25,27], who first developed PGM/ γ - Al_2O_3 based HC-SCR catalysts successfully, observed a general NO_x conversion order of Pt (44%) > Pd (11%) > Rh (4%) at 200 °C. Even though the results identified Pt as the most active catalyst, there is a problem of predominant N_2O formation compared to the preferred reaction product N_2 and the more reactive NH_3 , reaching selectivities of 66–83% at 200–250 °C [28,29]. Contrarily, Rh/ Al_2O_3 catalysts with a slightly higher maximum performance temperature (250–300 °C) are found to show a much lower selectivity for N_2O ($\leq 30\%$) [28,29]. However, the NO conversion and N_2 -selectivity of the precious metal (PGM)-based catalysts are highly support-dependent as the studies of Burch and Millington [30] (Al_2O_3 vs. SiO_2) and Garcia-Cortés et al. [31] (Pt activity order: ZSM-5 \gg Al_2O_3 ; N_2 selectivity: Pt/ Al_2O_3 > Pt/ZSM-5) show.

Burch et al. [26,30,32] noted a correlation between the NO_x conversion and the propylene oxidation activity of PGM/alumina catalysts (PGM = Pt, Pd, Rh, Ir) and proposed a multi-step mechanism for the C_3H_6 -SCR reaction [26]. The proposed mechanism involves first a reduction of PGMO_x to metallic PGM by propylene (Equation (1)), activating the precious metal sites for NO adsorption. Afterwards, NO is either dissociatively adsorbed as N^* - and O^* -ad species or as NO^* -ad species depending on the temperature (Equation (2)). NO^* is the major form at low temperatures and favours the formation of undesired N_2O by a recombination of two NO^* -ad species (Equation (3)). Additionally, rival adsorption of O_2 onto the PGM (Equation (4)) counteracts with the NO_x reduction process and limits the NO dissociation as less activated PGM sites become accessible. The competition between NO and O_2 adsorption decreases with increasing temperatures leading to a more favoured N_2 production from adsorbed N^* -ad species (see equation 5) [26,33].



To reduce N_2O formation over Pt-based LNT catalysts at low temperatures there are two options: either conversion of the N_2O to N_2 or suppressing the C_3H_6 -SCR side reaction. The former option is quite challenging as the O_2 concentration is two orders of magnitude higher than that of N_2O concentration [34]. The most common catalysts investigated for this specific application are Rh-based due to their high N_2 selectivities [29,35], but they commonly suffer from a poor low-temperature activity as the light-off temperatures T_{50} (temperature of 50% conversion) are around 350 °C [34,36]. Centi et al. [34,36] investigated a zirconia catalyst with 1 wt.% of Rh for its N_2O conversion performance in different feed gas mixtures and observed a shift of T_{50} (~260 °C) to higher temperatures (T_{50} ~380–400 °C) in the presence of O_2 and H_2O due to catalyst deactivation. However, upon removal of O_2 and H_2O from the feed gas, the good performance (before adding O_2 and H_2O) at low temperatures could be retrieved [36,37]. The investigations of Beyer et al. [35] and Parres-Esclapez et al. [38] also showed a performance loss in N_2O conversion for 0.58 wt.% Rh/ Al_2O_3 (T_{50} = 341 °C) and 0.5 wt.% Rh/ $SrAl_2O_3$ (T_{50} \approx 300 °C), caused by the presence of O_2 .

The second approach of SCR reaction inhibition can be achieved with a reduction of available propylene by oxidation. Again, supported noble metal catalysts possess a remarkable ability for the oxidation of hydrocarbons and CO at low temperatures. Palladium is the most common commercially used precious metal [39], for example, in the compositions Pd/ CeO_2 [40,41], Pd/ Al_2O_3 [42] and Pd/ CeO_2 - Al_2O_3 [42]. The survey of Shen et al. [41] displays a strong relation between the C_3H_6 and CO light-off temperatures and the loaded Pd content. It was shown that the light-off temperature $T_{50}(C_3H_6)$ shifts from around 225 °C to 140 °C upon increasing the Pd loading from 1 to 7 wt.% [41]. The same shift was observed for the CO oxidation T_{50} values, which are commonly at lower temperatures than for propylene oxidation (e.g., $T_{50}(CO)$ at ~200 °C for 1 wt.% Pd). Even though Faria et al. [43] proposed CeO_2 to enhance the oxidation ability of Pd/ Al_2O_3 due to a better precious metal dispersion, Guimarães et al. [42] observed a T_{50} shift to higher temperatures with the incorporation of ceria ($T_{50}(Pd/Al_2O_3)$: ~375 °C and $T_{50}(Pd/CeO_2/Al_2O_3)$: ~490 °C). However, it must be pointed out that both catalysts were pre-treated differently.

Infiltration composites with 20 wt.% loadings of B-site substituted lanthanum strontium ferrates ($La_{0.5}Sr_{0.5}Fe_{1-x}M_xO_{3-\delta}$ M = Nb, Ti, Zr) on an alumina support showed promising NO_x storage capacities (NSC) for the substituting elements Nb, Ti and Zr under laboratory testing conditions [44]. Depending on the perovskite composition a maximal NSC of around 120 to 164 $\mu\text{mol/g}$ was measured in the temperature range from 250 °C to 350 °C. Hereby, an increasing maximum NSC and a temperature-dependent shift to lower temperatures are found in the order of Nb < Ti < Zr [44].

The main focus of this study is to investigate nitrous oxide formation on 2.5 wt.% Pt/20 wt.% $La_{0.5}Sr_{0.5}Fe_{1-x}M_xO_{3-\delta}/Al_2O_3$ (M = Nb, Ti, Zr)-based lean NO_x trap catalysts in the lean operation mode. After determining the underlying mechanism of formation in the presence of CO and C_3H_6 reductives [23], different approaches to reduce or avoid nitrous oxide formation have been examined. The first approach considers an additional precious metal coating of 0.125 wt.% Rh obtained via incipient wetness impregnation onto the LNT catalyst in order to increase the number of active NO_x oxidation and reduction sites on the catalyst surface as well as the N_2 selectivity. The second approach comprises the usage of an oxidation catalyst (2 wt.% Pd/20 wt.% CeO_2/Al_2O_3) deposited on top of the LNT material in a two-layer configuration within the reactor to decrease the reductive concentrations before passing through the LNT catalyst.

2. Results

2.1. N_2O Formation on $Pt/La_{0.5}Sr_{0.5}Fe_{1-x}M_xO_{3-\delta}/Al_2O_3$ (M = Nb, Ti, Zr; x = 0.25 or 0.5) during Lean Operation Conditions

The temperature-dependent NO_x storage capacity investigations were carried out up to the NO_x saturation of the catalysts in order to determine not only the maximum storage capacity of the materials but also any possible side reactions, e.g., N_2O or NH_3 formation. Figure 1 shows the detected temperature-dependent N_2O formation curves

for 2.5 wt.% Pt/20 wt.% $\text{La}_{0.5}\text{Sr}_{0.5}\text{Fe}_{0.5}\text{Ti}_{0.5}\text{O}_3/\text{Al}_2\text{O}_3$ (LSFT_Pt), 2.5 wt.% Pt/20 wt.% $\text{La}_{0.5}\text{Sr}_{0.5}\text{Fe}_{0.75}\text{Nb}_{0.25}\text{O}_3/\text{Al}_2\text{O}_3$ (LSFN_Pt) and 2.5 wt.% Pt/20 wt.% $\text{La}_{0.5}\text{Sr}_{0.5}\text{Fe}_{0.5}\text{Zr}_{0.5}\text{O}_3/\text{Al}_2\text{O}_3$ (LSFZ_Pt) along with that for the reference catalyst 2.5 wt.% Pt/20 wt.% $\text{BaO}/\text{Al}_2\text{O}_3$ (BaO_Pt). The general curve trend is that a profound increase in the amount of N_2O formed at low temperature (up to ~19 to 25 ppm at 250 °C), is followed by a profound decline at temperatures above 350 °C to an almost zero level. These results demonstrate similar behaviour for the perovskite-type oxide-based infiltration composites as is known for other (earth-) alkaline-based LNT catalysts [9,11,16,45]. Nevertheless, a small difference is found between the performance of LSFN_Pt and that of the other catalysts. The Nb-containing catalyst displays a much lower activity as significantly lower N_2O formation values are found in the temperature range of 250–300 °C when compared to values found for the other catalysts.

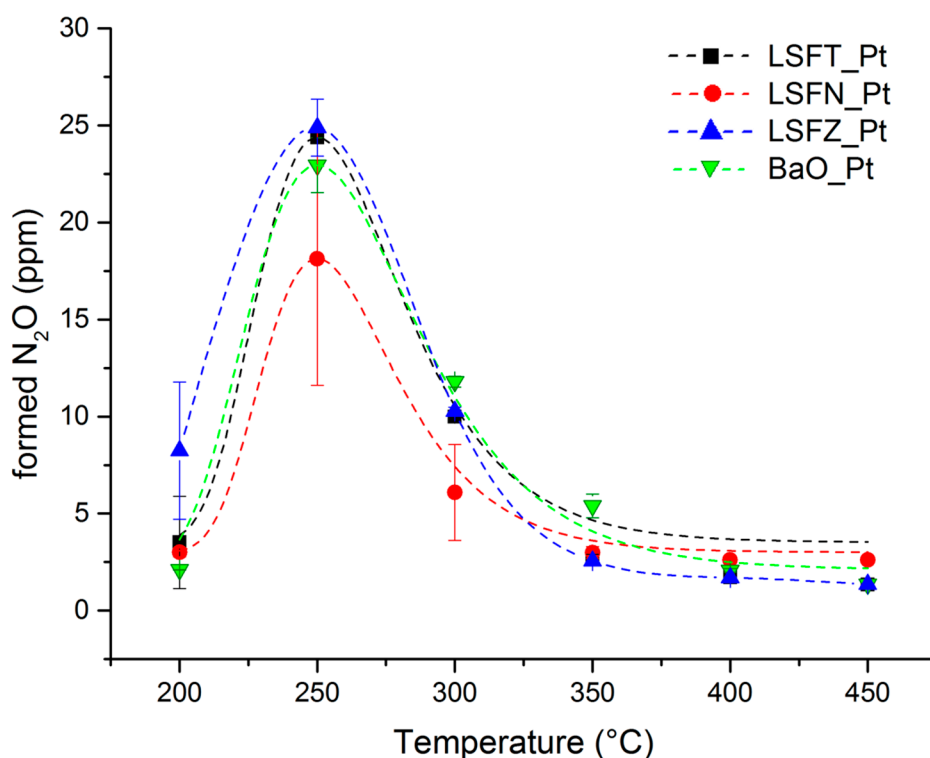


Figure 1. Temperature dependence of N_2O formation during the adsorption phase at lean operation conditions for different Pt-coated perovskite-based LNT catalysts. Data for the reference catalyst 2.5 wt.% Pt/20 wt.% $\text{BaO}/\text{Al}_2\text{O}_3$ (BaO_Pt) are given for comparison.

To examine the impact of reductive gases CO and C_3H_6 on the N_2O formation in more detail, additional temperature-dependent NO_x storage measurements were carried out under different synthetic exhaust gas compositions (Table 1). These experiments were conducted only for the LSFZ_Pt. Corresponding results are given in Figure 2.

Table 1. Exhaust gas compositions used in C_3H_6 -SCR experiments.

Components	synthetic Exhaust Gas Mixtures (Balanced with N_2)		
	lean	w/o_CO	w/o_ C_3H_6
CO_2	9 vol.%	9 vol.%	9 vol.%
H_2O	9 vol.%	9 vol.%	9 vol.%
O_2	6.5 vol.%	6.5 vol.%	6.5 vol.%
CO	500 ppm	-	500 ppm
C_3H_6	200 ppm	200 ppm	-
NO	500 ppm	500 ppm	500 ppm

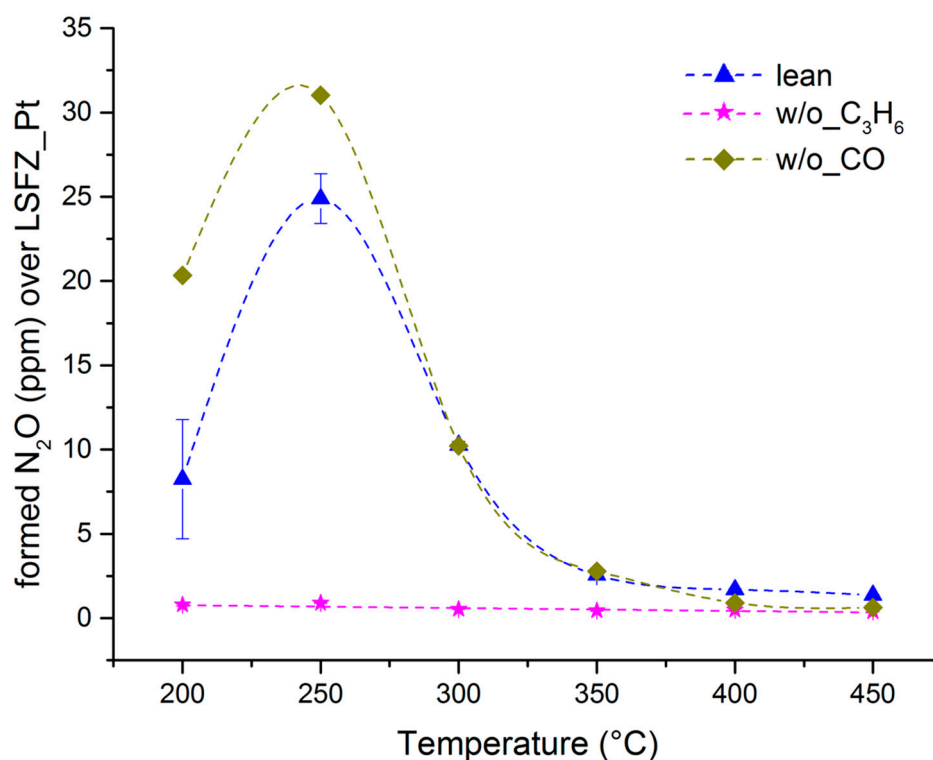


Figure 2. Temperature dependence of N₂O formation over LSFZ_Pt in different synthetic exhaust gas compositions. Feed gas compositions are listed in Table 1.

Whereas the exhaust gas mixture without CO (labelled w/o_CO) shows a curve progression analogous to that of the lean gas mixture (i.e., with CO and C₃H₆), the feed gas without propylene (labelled w/o_C₃H₆) shows a completely temperature-independent behaviour with a constant, almost negligible N₂O formation of around 1–2 ppm. The results clearly reveal a N₂O evolution dependency on the presence of propylene only, and so do verify a propylene-SCR mechanism. Furthermore, when comparing the progression curves of the lean exhaust gas and that without CO, a higher N₂O evolution at 200 °C and 250 °C is observed for the latter. These results suggest that CO counteracts the undesired N₂O formation mechanism at low temperatures.

2.2. Impact of Rh on the NO_x Storage Capacity and N₂O Evolution of the Infiltration Composites

Rhodium catalysts are most effective in reducing N₂O emissions due to their excellent N₂O decomposition properties at temperatures above 300 °C [34–36]. However, Hamada [29] observed a slight C₃H₆-SCR activity for Rh/Al₂O₃ in a net oxidising atmosphere already at 200 and 250 °C. Due to this activity, the addition of rhodium to the platinised infiltration composites (2.5 wt.% Pt/20 wt.% La_{0.5}Sr_{0.5}Fe_{1-x}M_xO_{3-δ}/Al₂O₃) seems to be a possibility to reduce N₂O emission at 250 °C, corresponding to the temperature of maximal N₂O formation, by a more selective catalytic reduction reaction (see Figure 1).

Since Abduhlhamid et al. [20] reported a low catalytic activity of Rh in NO oxidation, a combined Pt-Rh coating on the infiltration composites was used to maintain a good NSC, while decreasing the N₂O evolution. According to the commonly commercially used Pt to Rh ratio, the Rh amount was set to 0.125 wt.%, leading to a Pt-Rh ratio of 1:0.05. Figure 3 compares obtained data for the NSC and N₂O formation of as-prepared LSFT_Pt and LSFT_PtRh. Starting with a comparison of the NSC (Figure 3A) of the bare Pt-coated and that of mixed Pt-Rh coated samples, a general shift of the adsorption curve by 50 °C towards higher temperatures occurs due to the addition of 0.125 wt.% Rh. As a result, the Pt-Rh combination shows a higher NSC than bare Pt in the range of 300–450 °C.

Additionally, the maximum storage temperature increases from 142 $\mu\text{mol/g}$ for LSFT_Pt (250 $^{\circ}\text{C}$) to 151 $\mu\text{mol/g}$ for LSFT_PtRh (300 $^{\circ}\text{C}$). The expectation that N_2O formation for LSFT_PtRh is decreased with slightly increasing the NSC is refuted by the results shown in Figure 3B. Here it can be seen that with additional Rh coating, a higher N_2O formation over the entire temperature range occurs for LSFT_PtRh. While the average amounts of N_2O formed in the moderate to high-temperature range continue to converge, ending at values of 1–3 ppm, the difference in the low-temperature range is substantial. While the difference is about 15 ppm at 200 $^{\circ}\text{C}$, it is reduced to 2 ppm at temperatures above 250 $^{\circ}\text{C}$.

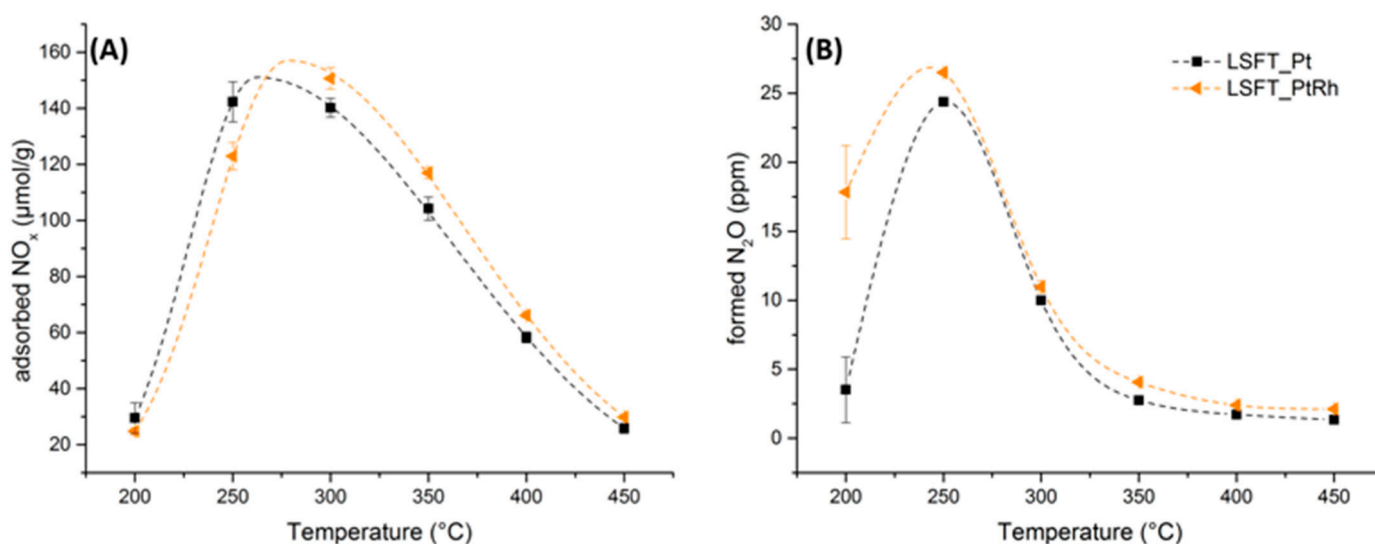


Figure 3. Temperature dependence of the (A) NO_x storage capacity and (B) N_2O formation of LSFT_PtRh. Data for LSFT_Pt from [44] also shown for comparison.

2.3. Performance Study of a Mixed Composition of 80 vol.% LNT (Bottom) and 20 vol.% Oxidation Catalyst (Top)

The second approach to avoid N_2O evolution deals with the oxidation of propylene before it reaches the LNT catalyst. Here, the choice for the oxidation catalyst was set to 2 wt.% Pd/20 wt.% $\text{CeO}_2/\text{Al}_2\text{O}_3$ (Ce_Pd) as this composition has advantageous properties for both oxidation of propylene and CO. Next to the outstanding and well-established oxidation properties of Pd, CeO_2 is expected to promote the oxidation ability of the catalyst due to the easy change between Ce^{3+} and Ce^{4+} oxidation states [46,47]. Furthermore, former studies on combined Pd and CeO_2 -based oxidation catalysts showed a more homogeneously dispersed palladium coating and thus sinter stable Pd particles [43] and a performance shift to lower temperatures depending on the coated Pd amount [41].

In this experiment first, the activity of the Ce_Pd catalyst composition for CO and C_3H_6 oxidation has been investigated in separate (w/o_CO and w/o_ C_3H_6) and co-feed (full lean gas mixture; see Table 1) experiments and the resulting light-off curves are shown in Figure 4. The CO oxidation occurs in the temperature range of 70–185 $^{\circ}\text{C}$ for the separate (w/o_ C_3H_6) feed mixture and the propylene oxidation is observed between 185 and 280 $^{\circ}\text{C}$ for the feed gas mixture without CO. With these feed conditions the T_{50} values are estimated to be 157 and 252 $^{\circ}\text{C}$ for CO and propylene, respectively. Due to the co-feed of 500 ppm CO and 200 ppm C_3H_6 , the light-off curves of both reducing gases have converged and show similar start and end temperatures for the oxidation curves. In principle, the light-off curve of CO was shifted on average by 40 $^{\circ}\text{C}$ to higher temperatures ($T_{50}(\text{CO}) = 191$ $^{\circ}\text{C}$), while the C_3H_6 light-off curve was shifted by around 20 $^{\circ}\text{C}$ to lower temperatures ($T_{50}(\text{C}_3\text{H}_6) = 232$ $^{\circ}\text{C}$) than in the separate feed experiment. With that, the results of the full lean gas feed experiment indicate a kind of promoting role of CO for C_3H_6 oxidation and an improved performance in the low-temperature range of 200–300 $^{\circ}\text{C}$.

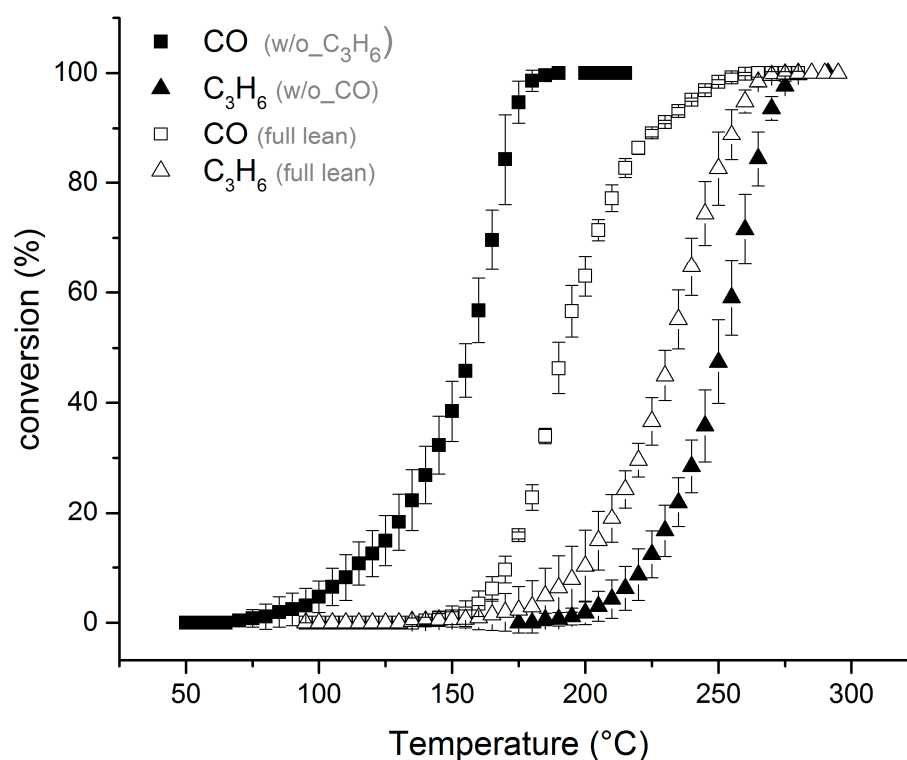


Figure 4. Separate CO and propylene (filled symbols) and full lean feed (CO + C₃H₆; open symbols) oxidation measurement data as a function of temperature using 2 wt.% Pd/20 wt.% CeO₂/Al₂O₃ (Ce_Pd) as oxidation catalyst. The compositions of the feed gas mixtures are given in Table 1.

In the following, the reactor filling changed to a layered two component system. Therefore, 2 mL (20 vol.%) Ce_Pd was fixed on top of 8 mL NO_x storage active infiltration composite (see Figure 5A), keeping the reactor filling constant at a total filling volume of 10 mL, to effectively change the gas mixture by the conversion of propylene and CO to CO₂ and water before entering the LNT catalyst (80 vol.%).

Figure 5B reveals the temperature-dependent NSC for the single LSFZ_Pt sample and the layered Ce_Pd-LSFZ_Pt system. The comparison shows that the layered catalyst system keeps the general Gaussian-type curve progression with a maximum at 250 °C as already observed for the pure LSFZ_Pt sample. The maximal performance for bare LNT and the layered catalyst system are similar, as the average values are 171 μmol/g and 176 μmol/g. However, by the addition of the oxidation catalyst the stored NO_x amount is increased at temperatures above 250 °C until 400 °C, resulting in a performance enhancement of 15–22%. Due to the increase an almost equal performance at 300 °C (169 μmol/g) than for 250 °C occurs thereby broadening the high-performance window of the LNT catalyst. In conjunction with the increased NO_x storage capacity, a decrease in the formed N₂O amount can be observed in Figure 5C due to the addition of the oxidation catalyst. The decrease occurs in the range of 200–350 °C and accounts for between 60% (200 °C) and 13% at the maximum evolution temperature.

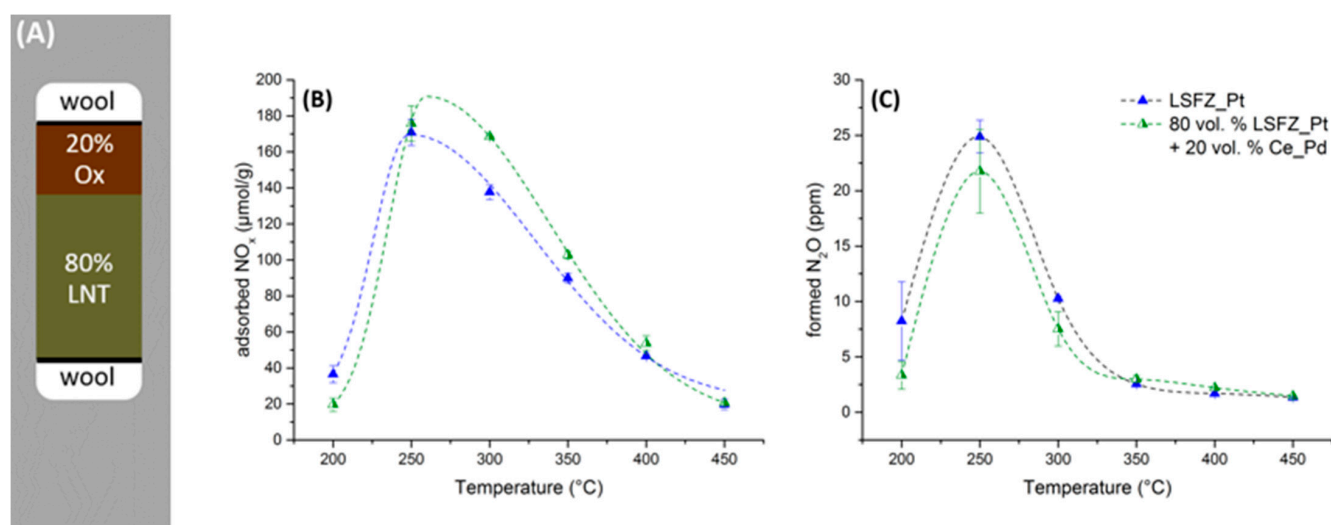


Figure 5. (A) Scheme of the filling constitution for the top-layered oxidation catalyst-LNT combination. Comparison of the temperature dependent NO_x storage capacity (B) and N₂O formation (C) for LSFZ_Pt (▲, from reference [44]) and a catalyst combination of 80 vol.% LSFZ_Pt covered with 20 vol.% of Ce_Pd (▼).

3. Discussion

3.1. Catalyst Characterisation

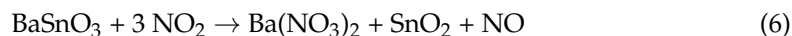
The infiltration composites Pt/La_{0.5}Sr_{0.5}Fe_{0.5}Ti_{0.5}O_{3-δ}/Al₂O₃ (LSFT_Pt), Pt/La_{0.5}Sr_{0.5}Fe_{0.75}Nb_{0.25}O_{3-δ}/Al₂O₃ (LSFN_Pt) and Pt/La_{0.5}Sr_{0.5}Fe_{0.5}Zr_{0.5}O_{3-δ}/Al₂O₃ (LSFZ_Pt) were already introduced as potential LNT materials in a previous work and extensively characterised by BET, X-ray diffraction (XRD), selected area electron diffraction (SAED) and transmission electron microscopy (TEM) [44]. The analysis of the specific surface areas (SSA) of the infiltration composites showed that with the use of the incipient wetness impregnation method the loss of the SSA, starting from γ-Al₂O₃, could be kept low despite the multi-step synthesis route. As a result, an SSA between 99 and 106 m²/g was measured for the three nanocomposite compositions at a perovskite loading of 20 wt.% (equivalent prepared Pt/BaO/Al₂O₃ displayed an SSA of 80 m²/g). The varying specific surface areas depending on the substituting B-site cations in the perovskites could be explained by the different crystallisation behaviour due to the material composition. SAED measurements performed on the freshly prepared samples showed that the degree of crystallisation of the perovskites decreased in the order Ti > Nb > Zr, thus contradicting the decreasing order of the SSA. Furthermore, the successful in situ crystallisation of the expected perovskite compositions could be confirmed by additional ACOM-TEM images besides the SAED measurements. The results identified the infiltration composites as an ultrafine, uniform mixture of platinum, perovskite and alumina particles.

As the titanium-containing infiltration composite has shown the best crystallisation behaviour and NSC of all investigated infiltration composite mixtures, this material composition was chosen to investigate the impact of the additional 0.125 wt.% Rh coating. The resulting Pt/Rh/La_{0.5}Sr_{0.5}Fe_{0.5}Ti_{0.5}O_{3-δ}/Al₂O₃ (LSFT_PtRh) specimen shows the same well-matched perovskite composition due to the synthesis procedure using a perovskite precursor solution and has an SSA of 104 m²/g. Thus, the impact of the Rh-coating is marginal in the case of the morphological material properties.

3.2. N₂O Formation Investigations

Figure 1 shows the N₂O formation on perovskite-based lean NO_x trap (LNT) catalysts, and Pt/BaO/Al₂O₃ as a commonly known reference catalyst, under lean operation conditions as a function of temperature. Even though all examined materials show a similar Gaussian-type N₂O formation curve, a slight difference between LSFN_Pt and the other

specimen can be observed. A comparable behaviour pattern was also observed in the NSC experiments [44]. Assuming that the weaker NSC and N₂O evolutions depend on the perovskite composition, this behaviour could be due to a slowed ad-species spill-over from the precious metal to the storage material. Hodjati et al. [48] postulated a reversible opening mechanism for the storage of NO_x on ABO₃ perovskites (A = Ba, Ca, Sr; B = Sn, Ti, Zr) according to Equations (6) and (7).



In this case, the incorporation of the niobium cations may have led to a more stable perovskite lattice compared to Ti⁴⁺ (0.74 Å) [49] and Zr⁴⁺ (0.86 Å) [49] due to the equal ionic radii of Fe³⁺ (0.78 Å) [49] and Nb⁵⁺ (0.78 Å) [49]. The high redox stability of niobium oxides at temperatures below 900–1000 °C discussed by Gervasini [50] could also contribute to a lower crystal lattice opening probability. Under this assumption, the Nb-containing perovskite would be less reactive with respect to NO_x uptake and the ad-species would have to dwell longer on the platinum, thus inhibiting the overall activity of the precious metal with respect to NO_x storage and the N₂O forming side reaction.

By a following survey concerning different feed gas compositions (Figure 2), the underlying N₂O formation mechanism for our infiltration composites was clearly identified as a C₃H₆-SCR. Interestingly, a kind of inhibiting effect is observed, when CO and C₃H₆ are dosed together. The resulting lower N₂O evolution at 200 and 250 °C might be explained by an increased availability of active (reduced) Pt sites due to an additional PGM_x to PGM⁰ transformation by CO leading to more likely formed N*- and O*- ad-species and so a lower N₂O formation (see Equations (3) and (5)).

To the best of our knowledge, only Masdrag et al. [23] have so far investigated the influence of different reducing agents on N₂O formation on an LNT catalyst (Pt/CeO₂-ZrO₂) in lean operation. In their study, they defined a temperature-dependent reductive influence with CO > C₃H₆ ≈ 0 at 200 °C and C₃H₆ > CO ≈ 0 at 300 °C in lean operation mode. [23].

Hence, the catalyst investigations in our study and in the study of Masdrag et al. were conducted entirely in a net oxidising atmosphere (see Table 1), the Pt/La_{0.5}Sr_{0.5}Fe_xM_{1-x}O_{3-δ}/Al₂O₃ (M = Nb, Ti, Zr) infiltration composites show a pronounced N₂O formation by the C₃H₆-SCR reaction at 200 °C (see Figure 1), while Pt/CeO₂-ZrO₂ was completely inactive (reference [23], Figure 7A,B). It seems that the Pt particles (2.5 wt.%) in the composites can be reduced more effectively by C₃H₆ at low temperatures and O₂ excess than in the LNT catalyst studied by Masdrag et al. (2.12 wt.% Pt, CeO₂ content unknown) [23]. This difference can most likely be explained by the influence of the support materials and/or the Pt particle sizes (Pt particle size Masdrag et al.: 6.2 nm, this study: 2–4 nm).

Since the focus of C₃H₆-SCR catalyst studies is mostly on NO_x conversion and N₂ selectivity, no literature is known at this time that explicitly addresses the undesired N₂O formation as a function of different support materials and/or PGM particle size.

3.3. Attempts to Reduce N₂O Evolution

The first attempt to reduce the N₂O formation on LNT catalysts under lean conditions was the usage of an additional Rh coating on the infiltration composites. By the addition of 0.125 wt.% Rh the NO_x storage capacity above 300 °C is slightly improved (Figure 3A). Though an auxiliary effect of the Rh coating at higher temperatures seems to be plausible, as the studies of Kubiak et al. [51], Andonova et al. [52] and Castoldi et al. [53] showed appreciable NO oxidation abilities and NO_x storage capacities for Rh-based BaO/Al₂O₃ catalysts above 350 °C. Figure 3B compares the N₂O evolution on LSFT_Pt and LSFT_PtRh. The observed N₂O formation increase caused by the Rh addition could be related to an interplay between the generally high light-off temperatures for NO oxidation and N₂O decomposition of Rh-based catalysts on the one hand, and the slight NO_x adsorption

capacity at low temperatures proceeding via the nitrite route on the other hand. The latter usually proceeds by a subsequent transfer of activated oxygen from the PGM to the storage material, allowing the adsorption of NO in the form of nitrite adsorbents. Consequently, Kubiak et al. [51] observed a low NO_x adsorption of 0.106 mmol/g for Rh/BaO/Al₂O₃ at 150 °C in 1000 ppm NO + 3 vol.% O₂ balanced with helium. Due to the feed gas composition used here, which contains reducing agents during the lean phase (propylene and CO), it can be assumed that the nitrite pathway is inhibited by the partial reduction of the noble metal sites. Thus, the available amount of activated oxygen would decrease and consequently lead to the recombination of the weakly bound NO-ad species at the PGM and storage material sites and the formation of N₂O. However, the dramatic increase of about 500% of evolving N₂O at 200 °C cannot only be related to additional N₂O formation over 0.125 wt.% Rh, hence indicating a strong impeding interaction between the Rh and Pt concerning NO oxidation at low temperatures in the presence of reductives.

The second attempt deals with the use of a layered oxidation and LNT (ratio 1:4) catalyst as illustrated in Figure 5A. The chosen oxidation catalyst 2 wt.% Pd/20 wt.% CeO₂/Al₂O₃ (Ce_Pd) showed a promising oxidation ability for propylene and CO in separate and co-feed experiments (Figure 4), thus seeming able to suppress N₂O production via SCR reaction. In general, Ce_Pd showed a similar performance compared to the results of Shen et al. [41] and Burch and Millington [30], who observed a complete activation of their investigated Pd/CeO₂-ZrO₂ and Pd/Al₂O₃ catalysts for propylene oxidation in a temperature range of around 125 °C (T₅₀ = 203 °C) and 100 °C (T₅₀ = 250 °C). The oxidation activity for both- CO and C₃H₆- raises from 0 to 100% by a temperature increase of around 100 °C in all feed gas experiments. Interestingly, due to the co-feed of CO and propylene, a convergence of the light-off curves (LO) was observed, shifting the CO-LO to higher and the C₃H₆-LO to lower temperatures. Similar experiments on Pt/Al₂O₃ [54–56] or Pt/CeO₂ [57] oxidation catalysts have shown that under co-feed conditions both LO curves commonly shift to higher temperatures as the two reducing gases compete for the active sites and thus inhibit the oxidation of the other gas. Only Lang et al. [58] observed a similar behaviour for 1 wt.% Pd/CeO₂-ZrO₂ as for the herein investigated 2 wt.% Pd/20 wt.% CeO₂/Al₂O₃ with a more pronounced approximation of the light-off curves for CO and propylene (T₅₀(CO) shift from 164 to 229 °C and T₅₀(C₃H₆) shift from 226 to 232 °C) and an improved C₃H₆ conversion at temperatures above ~240 °C (T₈₅(C₃H₆) ≈ 261 °C shifts to ~250 °C) due to the CO and propylene co-feed. Lang et al. [58] explained this behaviour by a possible alternating oxidation mechanism and/or lower activation barriers due to the available ceria compared to alumina-based catalysts (CO reaction order Pd/Al₂O₃: 1st order and Pd/CeO₂-ZrO₂: 0th order). Related to the mentioned literature, we presume a combination of both theories to be the reason for the observed curve shifts due to the CO and C₃H₆ co-feed. The observed shift of the CO-LO to higher temperatures seems to be caused by the general inhibition of the CO oxidation by competing propylene molecules and/or oxidation intermediates for the active catalyst sites. Instead, the promotion of the C₃H₆ oxidation by co-dosed CO might be explained by either an alternating oxidation mechanism dependent on the Pt supporting oxides or by more available Pt⁰ sites due to the prior or simultaneously elapsing CO oxidation consuming the oxygen species bound on the precious metal (PtO_x) [56]. Hazlett et al. [56] already observed that the addition of propylene to the feed gas resulted in a strong increase in multiple precious metal-bound surface species (triple bound adsorbates, carbonyl and dicarbonyl species) on Pt- and Pd-based alumina catalysts competing with the single precious metal-bound CO. In this case, C₃H₆ needs, on average, three times the amount of available active catalyst sites (Pt⁰) compared to CO for the oxidation reaction, which is commonly described as a Langmuir-Hinshelwood mechanism using surface co-adsorbed reactants [54]. However, the results in Figure 4 reveal that the catalyst offers the necessary oxidation activity in the desired temperature range of 200–500 °C to be used as an oxidation catalyst top layer for our approach to reduce C₃H₆ concentrations in the feed gas of the LNT catalyst. The resulting NO_x storage and N₂O evolution curves for the layered system are compared to the bare

LNT material (LSFZ_Pt) in Figure 5B,C. Due to the addition of Ce_Pd an increase of 15–22% of the NO_x storage capacity (NSC) in the temperature range of 250–400 °C is obtained. In parallel to the NSC enhancement, a N₂O formation decrease can be observed at 200 to 350 °C. The results thus show a N₂O evolution diminishment of 13–60% in the general N₂O formation window. Consequently, an oxidation catalyst layered on top of the LNT seems to be a suitable means to suppress N₂O formation during the lean storage phase of the LNT due to a competing propylene-SCR. Nevertheless, nitrous oxide emissions were not reduced to a zero level which might be caused by the chosen configuration with only a small oxidation catalyst layer on top of the LNT materials. To enhance the effect on NSC and N₂O evolution, the optimal thickness of the oxidation catalyst has to be found.

4. Materials and Methods

4.1. Lean NO_x Trap Catalyst Preparation

All investigated LNT storage materials were synthesised by a four-step synthesis pathway using incipient wet impregnation (IWI) processes ending up with a milling and granule formation step to give the materials the necessary geometry for the NO_x adsorption tests. A detailed description of each single preparation step can be found elsewhere [44].

In brief, firstly a citric acid stabilised aqueous perovskite precursor solution for each of the three investigated perovskite compositions La_{0.5}Sr_{0.5}Fe_{0.75}Nb_{0.25}O₃, La_{0.5}Sr_{0.5}Fe_{0.5}Ti_{0.5}O₃ and La_{0.5}Sr_{0.5}Fe_{0.5}Zr_{0.5}O₃ was prepared. Therefore, the starting materials La(NO₃)₃·6H₂O (Alfa Aesar, Karlsruhe, Germany, 99.9%), Sr(NO₃) (Alfa Aesar, Karlsruhe, Germany, ≥99.0%), Fe(NO₃)₃·9H₂O (Alfa Aesar, Karlsruhe, Germany, ≥98.0%) were dissolved in distilled water and stabilised with citric acid (VWR chemicals, Pennsylvania, USA, metal: citric acid 1:3). The varying fourth ingredient was added as a highly concentrated (around 5 wt.% transition metal load) complex solution, gained from titanium(IV) *iso*-propoxides (Alfa Aesar, Karlsruhe, Germany), zirconium(IV) *n*-propoxide in *n*-propanole (70 wt.%, Alfa Aesar, Karlsruhe, Germany) or ammonium niobate(V) oxalate hydrates (Sigma Aldrich, Taufkirchen, Germany) complexed with citric acid, to yield a perovskite precursor solution of either 1:1:1:1 or 1:1:1.5:0.5 stoichiometry. Secondly, a commercial alumina powder (Puralox TH 100/150/L4, Sasol, Hamburg, Germany) was infiltrated via IWI with the precursor solutions resulting in perovskite-alumina composites after subsequent thermal treatment. Exemplarily, 100 g of the two-component composite with a 20 wt.% Ti containing perovskite loading were prepared by the infiltration of 120 mL precursor solution into 80 g alumina. After calcination of the overnight-dried perovskite-alumina composites (100 °C/h, 700 °C, 5 h), additional 2.5 wt.% platinum was coated on the material via IWI using an aqueous solution of H₂Pt(OH)₆ (abcr GmbH, Karlsruhe, Germany) and (CH₃)₄NOH·5H₂O (Alfa Aesar, Karlsruhe, Germany) in a proportion of 1:2. The coated infiltration composite powders were dried at 120 °C and finally calcined at 550 °C for 1 h (175 °C/h). After milling, granules in fractions of 1.5 to 2.5 mm were formed. The resulting catalysts were abbreviated with LSFT, LSFN or LSFZ related to the perovskite-type oxide constructing elements followed by the platinum element symbol. Exemplarily, 2.5 wt.% platinum on 20 wt.% La_{0.5}Sr_{0.5}Fe_{0.5}Ti_{0.5}O_{3-δ}/Al₂O₃ is abbreviated as LSFT_Pt.

The platinised titanium perovskite-type oxide-based catalyst was further impregnated with 0.125 wt.% rhodium by another IWI coating step. Therefore 50 g of the LSFT_Pt composite was infiltrated with a solution of 0.174 g Rh(NO₃)₃ hydrate (36 wt.% Rh content, Merck, Darmstadt, Germany) dissolved in 60 mL distilled water. The wet powder was dried at 140 °C and calcined at 550 °C for 1 h using a heating rate of 175 °C/h. Afterwards, an analogous milling and granulation procedure as for the Pt only containing infiltration composites was carried out to examine their NSC and N₂O evolution at lean conditions. The composite 0.125 wt.% Rh-2.5 wt.% Pt on 20 wt.% La_{0.5}Sr_{0.5}Fe_{0.5}Ti_{0.5}O_{3-δ}/Al₂O₃, was abbreviated as before but with the additional element symbol of rhodium resulting in LSFT_PtRh.

Additionally, a comparable 2.5 wt.% Pt/20 wt.% BaO/Al₂O₃ sample, condensed as BaO_Pt, was synthesised by IWI. A 100 g synthesis batch was prepared by impregnating

80 g alumina (Puralox TH 100/150/L4, Sasol, Hamburg, Germany) with an aqueous barium solution. For the latter 33.32 g $\text{Ba}(\text{CH}_3\text{COO})_2$ were dissolved in 120 mL distilled water. After impregnation and homogenisation, the wet powder was dried at 120 °C overnight and calcined at 700 °C for 3 h. Similar to all former specimen, the composite powder was additionally coated with 2.5 wt.% Pt, grounded and formed to granules.

4.2. Oxidation Catalyst Preparation

50 g of the used 2 wt.% Pd/20 wt.% $\text{CeO}_2/\text{Al}_2\text{O}_3$ oxidation catalyst was prepared via incipient wetness impregnation. First, 28 g of an aqueous $(\text{NH}_3)_4\text{Pd}(\text{NO}_3)_2$ solution (10 wt.% Pd content, Alfa Aesar, Karlsruhe, Germany) were further diluted with 32 mL distilled water. The created solution was infiltrated on 49 g of commercial 20 wt.% ceria containing alumina powder (Puralox SCFa-160/Ce20, Sasol, Hamburg, Germany). After drying at 140 °C overnight, a final calcination was performed at 550 °C for 1 h using a heating rate of 175 °C/h. The catalyst powder was milled down and granulated in the way as described before. The catalyst is abbreviated as Ce_Pd.

4.3. NO_x Adsorption and N_2O Evolution Measurements as a Function of Temperature

Temperature-dependent NO_x adsorption measurements were performed in a laboratory exhaust gas test bench under constant lean conditions representing the exhaust gas composition on a lean burn engine at a lambda situation of $\lambda = 1.5$. In general, this was realised by the lean gas mixture (see Table 1) and a gas hourly space velocity set to 80,000 h^{-1} . In order to examine the dependence of the N_2O formation on the dosed reductives, additional NO_x storage measurements with altered gas compositions, either without CO (w/o_CO) or without propylene (w/o_C₃H₆) were dosed (see Table 1). A more detailed description of the used test bench could be found elsewhere [44]. In brief, all gas concentrations were controlled by dynamic gas flow controller (MFC) of type 5850 from Brooks Instrument, LLC (Hatfield, PA, USA). The inert carrier gas stream of N_2 , O_2 and CO_2 was heated up to 200 °C before the water vapour was added, dosed by a gear type pump from GATHER Industrie (Wülfrath, Germany) and vaporised by an evaporator from LINSEIS Messgeräte (Selb, Germany). The gas mixture was passed through a furnace (DLERH, Horst, Lorsch, Germany) and heated to the respective adsorption temperature (200–450 °C in 50 °C steps) in advance. The further gas flow towards the reactor with the sample was carried out in heated pipes and shortly before entering the reactor the reactive gases NO, CO and propylene were mixed into the carrier gas stream. To guarantee a constant temperature during the measurement, the titanium reactor was wrapped with a heat jacket (Horst, Lorsch, Germany) and the temperature was controlled by thermocouples (NiCrNi) at two points in the gas stream. The first thermocouple was placed before the reactor entrance and the second directly within the sample. The sample holder was filled with 10 mL of granules of a sole infiltration composite (see Figure 6) or a top-layered 20 vol.% oxidation catalyst on 80 vol.% infiltration composite setting (see Figure 5A). In both cases, the catalysts were covered up- and downstream with 100 mg quartz wool and a titanium sieve. The outlet gas composition was analysed using a Fourier-transformed infrared spectrometer (FT-IR) of the type MultiGas 2030 from MKS instruments to monitor the formation of C- and N-containing components (e.g., NO, NO_2 , N_2O , propylene, CO) during the measurements.

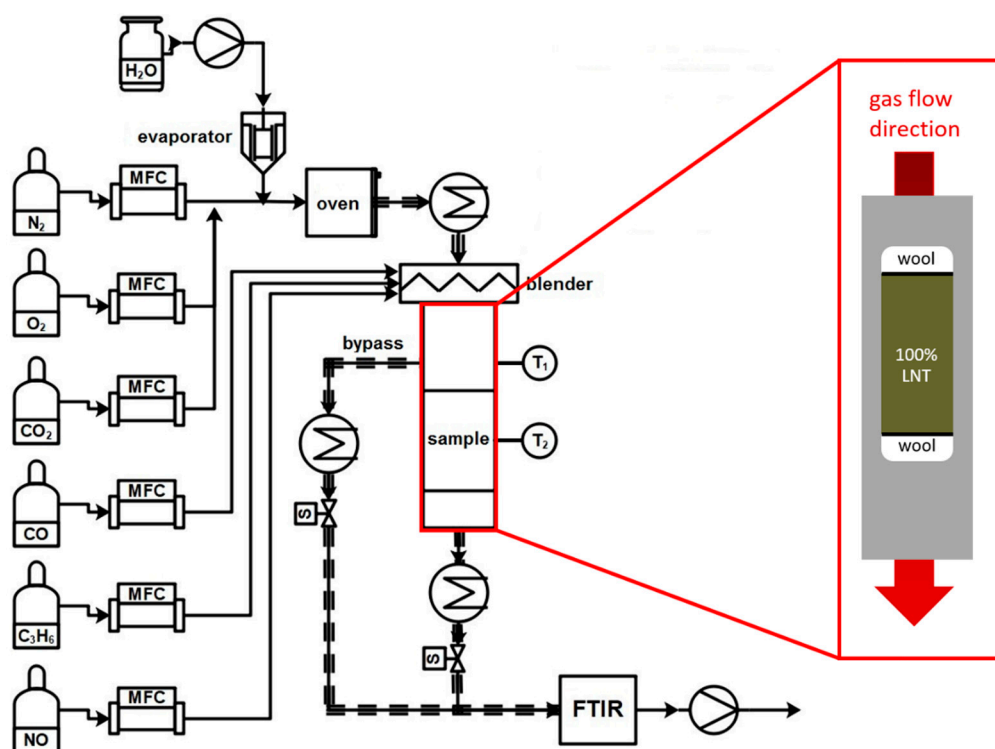


Figure 6. Technical drawing of the test bench and the reactor filling during only LNT catalyst examination experiments.

The NO_x storage capacity was measured between 200 and 450 °C in 50 °C steps by saturating the sample with NO_x . To control the gas composition before and after this adsorption phase, the gas mixture was switched via solenoid valves through a bypass, which directed the gas around the reactor. Afterwards, the stored NO_x was desorbed by heating up the sample to 550 °C within the same gas mixture but without NO dosing. Finally, the specific molar storage capacity was calculated from the NO_x desorption peak.

4.4. Propylene and CO Oxidation Measurements on 2 wt.% Pd/20 wt.% $\text{CeO}_2/\text{Al}_2\text{O}_3$ as a Function of Temperature

The measurements of the propylene and CO oxidising ability of the Ce20_Pd catalyst were carried out on the same laboratory gas test bench as the NO_x storage measurements (see Figure 6) at a gas hourly space velocity of 80,000 h^{-1} with three different feed gas compositions shown in Table 1. For the measurements, 2 mL of the catalyst was filled into the reactor and the gas mixtures were constantly passed through the sample. For propylene the temperature range of 165–295 °C and for CO the range between 60 and 215 °C was investigated. The heating rate in all cases was 2 °C/min. The cycles were repeated three times each. The resulting conversion curves are calculated with the following equations:

$$\text{CO conversion [\%]} = (\text{CO}_{\text{inlet}} - \text{CO}_{\text{outlet}}) / \text{CO}_{\text{inlet}} \times 100 \quad (8)$$

$$\text{C}_3\text{H}_6 \text{ conversion [\%]} = (\text{C}_3\text{H}_{6\text{inlet}} - \text{C}_3\text{H}_{6\text{outlet}}) / \text{C}_3\text{H}_{6\text{inlet}} \times 100 \quad (9)$$

5. Conclusions

This study focuses on the undesirable N_2O formation on newly developed Pt/ $\text{La}_{0.5}\text{Sr}_{0.5}\text{Fe}_{1-x}\text{M}_x\text{O}_3/\text{Al}_2\text{O}_3$ ($\text{M} = \text{Nb}, \text{Ti}, \text{Zr}$) lean NO_x trap (LNT) catalysts under laboratory gas test bench conditions. In addition to the investigations on the formation mechanism of the undesired by-product, which caused a decreased NO_x storage capacity (NSC) for the LNT materials, attempts were made to reduce these emissions. To this end, two approaches

were pursued, firstly an additive Rh coating on the LNT catalyst and secondly an oxidation catalyst-LNT layered system.

The mechanism of N_2O evolution was identified as a low-temperature C_3H_6 -SCR. Nitrous oxide formation occurred due to the competing partial reduction of PtO_x to Pt^0 by C_3H_6 during the general NO_x oxidation and storage procedure on LNT catalysts in net oxidising atmosphere. The investigations showed that even low concentrations of propylene (200 ppm), as generally present in lean exhaust gases, lead to high N_2O formation of 20 ppm on average at low temperatures.

The additional Rh coating on the $Pt/La_{0.5}Sr_{0.5}Fe_{0.5}Ti_{0.5}O_3/Al_2O_3$ nano composite resulted in a dramatic increase in N_2O formation in the range 200–250 °C. The comparison with the platinised nano composite sample leads to the assumption that this result can only be related to an additional N_2O formation at the Rh particles. It seems that the Rh nitrites route for NO_x storage is prevented by Pt^0 and Rh^0 particles. Thus the necessary oxygen spill-over is omitted causing a recombination of NO^* ad-species. Although the additional Rh coating is unsuitable for the reduction of N_2O formation, it should be mentioned that a slightly better NSC for the Pt and Rh coated sample was observed in the range of 300–450 °C.

In contrast, the catalyst installation with an oxidation catalyst connected upstream of the LNT showed promising results. With a replacement of 20 vol.% of the LNT by the oxidation catalyst (2 wt.% Pd/20 wt.% CeO_2/Al_2O_3), 13–60% less N_2O emissions were measured in the low temperature range. The results thus show that the oxidation of the propylene is the most effective way to reduce N_2O formation. Nevertheless, nitrous oxide formation could not yet be completely suppressed, which may be due to the catalyst configuration with a low oxidation catalyst content. To further improve the effectiveness of the oxidation catalyst, the palladium content and the layer thickness have to be optimised.

Author Contributions: The conceptualization was done by J.D. and S.I.E. All investigations were carried out by S.I.E. The necessary resources were provided by O.G. Supervision was carried out by J.D.; S.B.; H.J.M.B. and W.A.M. The original draft was prepared by S.I.E. and J.D.; S.B.; O.G.; H.J.M.B. and W.A.M. contributed to the writing-review and editing process. All authors have read and agreed to the published version of the manuscript.

Funding: This research was funded by the German Federal Ministry of Education and Research, Grant-No.: 13XP5042B.

Data Availability Statement: The data presented in this study are available on request from the corresponding author. The data are not publicly available due to the complexity of the analysis which needs guidance for reproduction.

Acknowledgments: Reprints from Ecker, S.I.; Dornseiffer, J.; Werner, J.; Schlenz, H.; Sohn, Y.J.; Sauerwein, F.S.; Baumann, S.; Bouwmeester, H.J.M.B.; Guillon, O.; Weirich, T.E.; Meulenberg, W.A. Novel low-temperature lean NO_x storage materials based on $La_{0.5}Sr_{0.5}Fe_{1-x}M_xO_{3-\delta}/Al_2O_3$ infiltration composites (M = Ti, Zr, Nb). *Appl. Catal. B Environ.* **2021**, *286*, 119919–119929 with permission from Elsevier.

Conflicts of Interest: The authors declare no conflict of interest.

References

1. Brijesh, P.; Sreedhara, S. Exhaust emissions and its control methods in compression ignition engines: A review. *Int. J. Automot. Technol.* **2013**, *14*, 195–206. [[CrossRef](#)]
2. Ayodhya, A.S.; Narayanappa, K.G. An overview of after-treatment systems for diesel engines. *Environ. Sci. Pollut. Res.* **2018**, *25*, 35034–35047. [[CrossRef](#)] [[PubMed](#)]
3. Zhu, J.; Wang, J.; Wang, J.; Dong, M.; Shen, M. Controlling N_2O formation during regeneration of NO_x storage and reduction catalysts: From impact of platinum-group metal type to rational utilization. *Phys. Chem. Chem. Phys.* **2017**, *19*, 32361–32372. [[CrossRef](#)]
4. Pieta, I.S.; Cortes-Reyes, M.; Larrubia, M.A.; Alemany, L.J.; Epling, W.S. Mechanistic Aspect of N_2O Formation Over Pt-Ba/ γ - Al_2O_3 Catalysts. *Top. Catal.* **2019**, *62*, 116–128. [[CrossRef](#)]
5. Irfan, M.F.; Goo, J.H.; Kim, S.D. Co_3O_4 based catalysts for NO oxidation and NO_x reduction in fast SCR process. *Appl. Catal. B Environ.* **2008**, *78*, 267–274. [[CrossRef](#)]

6. Koebel, M.; Elsener, M.; Kleemann, M. Urea-SCR: A promising technique to reduce NO_x emissions from automotive diesel engines. *Catal. Today* **2000**, *59*, 335–345. [CrossRef]
7. Takahashi, N.; Shinjoh, H.; Iijima, T.; Suzuki, T.; Yamazaki, K.; Yokota, K.; Suzuki, H.; Miyoshi, N.; Matsumoto, S.-I.; Tanizawa, T.; et al. The new concept 3-way catalyst for automotive lean-burn engine: NO_x storage and reduction catalyst. *Catal. Today* **1996**, *27*, 63–69. [CrossRef]
8. Huang, H.Y.; Long, R.Q.; Yang, R.T. The Promoting Role of Noble Metals on NO_x Storage Catalyst and Mechanistic Study of NO_x Storage under Lean-Burn Conditions. *Energy Fuel*. **2001**, *15*, 205–213. [CrossRef]
9. Mráček, D.; Kočí, P.; Marek, M.; Choi, J.-S.; Pihl, J.A.; Partridge, W.P. Dynamics of N₂ and N₂O peaks during and after the regeneration of lean NO_x trap. *Appl. Catal. B Environ.* **2015**, *166–167*, 509–517. [CrossRef]
10. Zhu, J.; Wang, J.; Wang, J.; Lv, L.; Wang, X.; Shen, M. New Insights into the N₂O Formation Mechanism over Pt-BaO/Al₂O₃ Model Catalysts Using H₂ As a Reductant. *Environ. Sci. Technol.* **2015**, *49*, 504–512. [CrossRef]
11. Dasari, P.; Muncrief, R.; Harold, M.P. Cyclic Lean Reduction of NO by CO in Excess H₂O on Pt–Rh/Ba/Al₂O₃: Elucidating Mechanistic Features and Catalyst Performance. *Top. Catal.* **2013**, *56*, 1922–1936. [CrossRef]
12. Yamazaki, K.; Suzuki, T.; Takahashi, N.; Yokota, K.; Sugiura, M. Effect of the addition of transition metals to Pt/Ba/Al₂O₃ catalyst on the NO_x storage-reduction catalysis under oxidizing conditions in the presence of SO₂. *Appl. Catal. B Environ.* **2001**, *30*, 459–468. [CrossRef]
13. Choi, J.-S.; Partridge, W.P.; Daw, C.S. Sulfur impact on NO_x storage, oxygen storage, and ammonia breakthrough during cyclic lean/rich operation of a commercial lean NO_x trap. *Appl. Catal. B Environ.* **2007**, *77*, 145–156. [CrossRef]
14. Kuroпка, J. Nitrous oxide emission- potential danger, balance and reduction possibilities. *Environ. Protect. Eng.* **2006**, *32*, 81–88.
15. Jabłońska, M.; Palkovits, R. It is no laughing matter: Nitrous oxide formation in diesel engines and advances in its abatement over rhodium-based catalysts. *Catal. Sci. Technol.* **2016**, *6*, 7671–7687. [CrossRef]
16. Bártová, Š.; Kočí, P.; Mráček, D.; Marek, M.; Pihl, J.A.; Choi, J.-S.; Toops, T.J.; Partridge, W.P. New insights on N₂O formation pathways during lean/rich cycling of a commercial lean NO_x trap catalyst. *Catal Today* **2014**, *231*, 145–154. [CrossRef]
17. Dong, M.; Wang, J.; Zhu, J.; Wang, J.; Wang, W.; Shen, M. Effects of Pd doping on N₂O formation over Pt/BaO/Al₂O₃ during NO_x storage and reduction process. *Front. Environ. Sci. Eng.* **2017**, *11*, 93–102. [CrossRef]
18. Regulations for Emissions from Vehicles and Engines. Available online: <https://www.epa.gov/regulations-emissions-vehicles-and-engines/final-rule-model-year-2012-2016-light-duty-vehicle> (accessed on 14 April 2021).
19. Ren, Y.; Harold, M.P. NO_x Storage and Reduction with H₂ on Pt/Rh/BaO/CeO₂: Effects of Rh and CeO₂ in the Absence and Presence of CO₂ and H₂O. *ACS Catal.* **2011**, *1*, 969–988. [CrossRef]
20. Abdulhamid, H.; Fridell, E.; Skoglundh, M. The reduction phase in NO_x storage catalysis: Effect of type of precious metal and reducing agent. *Appl. Catal. B Environ.* **2006**, *62*, 319–328. [CrossRef]
21. Abdulhamid, H.; Fridell, E.; Skoglundh, M. Influence of the type of reducing agent (H₂, CO, C₃H₆ and C₃H₈) on the reduction of stored NO_x in a Pt/BaO/Al₂O₃ model catalyst. *Top. Catal.* **2004**, *30*, 161–168. [CrossRef]
22. Nova, I.; Lietti, L.; Forzatti, P.; Prinetto, F.; Ghiotti, G. Experimental investigation of the reduction of NO_x species by CO and H₂ over Pt–Ba/Al₂O₃ lean NO_x trap systems. *Catal. Today* **2010**, *151*, 330–337. [CrossRef]
23. Masdrag, L.; Courtois, X.; Can, F.; Royer, S.; Rohart, E.; Blanchard, G.; Marecot, P.; Duprez, D. Understanding the role of C₃H₆, CO and H₂ on efficiency and selectivity of NO_x storage reduction (NSR) process. *Catal. Today* **2012**, *189*, 70–76. [CrossRef]
24. Amiridis, M.D.; Zhang, T.; Farrauto, R.J. Selective catalytic reduction of nitric oxide by hydrocarbons. *Appl. Catal. B Environ.* **1996**, *10*, 203–227. [CrossRef]
25. Hamada, H.; Kintaichi, Y.; Sasaki, M.; Ito, T.; Tabata, M. Transition metal-promoted silica and alumina catalysts for the selective reduction of nitrogen monoxide with propane. *Appl. Catal.* **1991**, *75*, L1–L8. [CrossRef]
26. Burch, R.; Millington, P. Selective reduction of nitrogen oxides by hydrocarbons under lean-burn conditions using supported platinum group metal catalysts. *Catal. Today* **1995**, *26*, 185–206. [CrossRef]
27. Hamada, H.; Kintaichi, Y.; Sasaki, M.; Ito, T.; tabata, M. Selective reduction of nitrogen monoxide with propane over alumina and HZSM-5 zeolite: Effect of oxygen and nitrogen dioxide intermediate. *Appl. Catal.* **1991**, *70*, L15–L20. [CrossRef]
28. Obuchi, A.; Ohi, A.; Nakamura, M.; Ogata, A.; Mizuno, K.; Ohuchi, H. Performance of platinum-group metal catalysts for the selective reduction of nitrogen oxides by hydrocarbons. *Appl. Catal. B Environ.* **1993**, *2*, 71–80. [CrossRef]
29. Hamada, H. Selective reduction of NO by hydrocarbons and oxygenated hydrocarbons over metal oxide catalysts. *Catal Today* **1994**, *22*, 21–40. [CrossRef]
30. Burch, R.; Millington, P.J. Selective reduction of NO_x by hydrocarbons in excess oxygen by alumina- and silica-supported catalysts. *Catal. Today* **1996**, *29*, 37–42. [CrossRef]
31. Garcia-Cortés, J.; Pérez-Ramirez, J.; Illán-Gómez, M.; Kapteijn, F.; Moulijn, J.; de Lecea, C.S.-M. Comparative study of Pt-based catalysts on different supports in the low-temperature de-NO_x-SCR with propene. *Appl. Catal. B Environ.* **2001**, *30*, 399–408. [CrossRef]
32. Burch, R.; Breen, J.; Meunier, F. A review of the selective reduction of NO_x with hydrocarbons under lean-burn conditions with non-zeolitic oxide and platinum group metal catalysts. *Appl. Catal. B Environ.* **2002**, *39*, 283–303. [CrossRef]
33. Sasaki, M.; Hamada, H.; Kintaichi, Y.; Ito, T. Role of oxygen in selective reduction of nitrogen monoxide by propane over zeolite and alumina-based catalysts. *Catal. Lett.* **1992**, *15*, 297–304. [CrossRef]

34. Centi, G.; Dall'Olio, L.; Perathoner, S. In situ activation phenomena of Rh supported on zirconia samples for the catalytic decomposition of N₂O. *Appl. Catal. A Gen.* **2000**, *194*, 79–88. [[CrossRef](#)]
35. Beyer, H.; Emmerich, J.; Chatziapostolou, K.; Köhler, K. Decomposition of nitrous oxide by rhodium catalysts: Effect of rhodium particle size and metal oxide support. *Appl. Catal. A Gen.* **2011**, *391*, 411–416. [[CrossRef](#)]
36. Centi, G.; Perathoner, S.; Vazzana, F.; Marella, M.; Tomaselli, M.; Mantegazza, M. Novel catalysts and catalytic technologies for N₂O removal from industrial emissions containing O₂, H₂O and SO₂. *Adv. Environ. Res.* **2000**, *4*, 325–338. [[CrossRef](#)]
37. Centi, G.; Dall'Olio, L.; Perathoner, S. Oscillating behavior in N₂O decomposition over Rh supported on zirconia-based catalysts: 2. Analysis of the reaction mechanism. *J. Catal.* **2000**, *194*, 130–139. [[CrossRef](#)]
38. Parres-Esclapez, S.; López-Suárez, F.; Bueno-López, A.; Illán-Gómez, M.; Ura, B.; Trawczynski, J. Rh–Sr/Al₂O₃ catalyst for N₂O decomposition in the presence of O₂. *Top. Catal.* **2009**, *52*, 1832–1836. [[CrossRef](#)]
39. Song, S.; Zhang, S.; Zhang, X.; Verma, P.; Wen, M. Advances in Catalytic Oxidation of Volatile Organic Compounds over Pd-Supported Catalysts: Recent Trends and Challenges. *Front. Mater.* **2020**, *7*, 1–14. [[CrossRef](#)]
40. Hadi, A.; Yaacob, I.I. Synthesis of PdO/CeO₂ mixed oxides catalyst for automotive exhaust emissions control. *Catal. Today* **2004**, *96*, 165–170. [[CrossRef](#)]
41. Shen, M.; Wei, G.; Yang, H.; Wang, J.; Wang, X. Different selections of active sites for CO, C₃H₆, and C₁₀H₂₂ oxidation on Pd/CeO₂ catalysts. *Fuel* **2013**, *103*, 869–875. [[CrossRef](#)]
42. Guimarães, A.L.; Dieguez, L.C.; Schmal, M. Surface Sites of Pd/CeO₂/Al₂O₃ Catalysts in the Partial Oxidation of Propane. *J. Phys. Chem. B* **2003**, *107*, 4311–4319. [[CrossRef](#)]
43. Faria, W.L.S.; Perez, C.A.C.; César, D.V.; Dieguez, L.C.; Schmal, M. In situ characterizations of Pd/Al₂O₃ and Pd/CeO₂/Al₂O₃ catalysts for oxidative steam reforming of propane. *Appl. Catal. B Environ.* **2009**, *92*, 217–224. [[CrossRef](#)]
44. Ecker, S.I.; Dornseiffer, J.; Werner, J.; Schlenz, H.; Sohn, Y.J.; Sauerwein, F.S.; Baumann, S.; Bouwmeester, H.J.M.; Guillon, O.; Weirich, T.E.; et al. Novel low-temperature lean NO_x storage materials based on La_{0.5}Sr_{0.5}Fe_{1-x}M_xO_{3-δ}/Al₂O₃ infiltration composites (M = Ti, Zr, Nb). *Appl. Catal. B Environ.* **2021**, *286*, 119919–119929. [[CrossRef](#)]
45. Kubiak, L.; Matarrese, R.; Castoldi, L.; Lietti, L.; Daturi, M.; Forzatti, P. Study of N₂O Formation over Rh- and Pt-Based LNT Catalysts. *Catalysts* **2016**, *6*, 36. [[CrossRef](#)]
46. Gorte, R.J.; Zhao, S. Studies of the water-gas-shift reaction with ceria-supported precious metals. *Catal. Today* **2005**, *104*, 18–24. [[CrossRef](#)]
47. Wieder, N.L.; Cargnello, M.; Bakhmutsky, K.; Montini, T.; Fornasiero, P.; Gorte, R.J. Study of the Water-Gas-Shift Reaction on Pd@CeO₂/Al₂O₃ Core-Shell Catalysts. *J. Phys. Chem. C* **2011**, *115*, 915–919. [[CrossRef](#)]
48. Hodjati, S.; Vaezzadeh, K.; Petit, C.; Pitchon, V.; Kiennemann, A. Adsorption/desorption of NO_x process on perovskites: Performances to remove NO_x from a lean exhaust gas. *Appl. Catal. B Environ.* **2000**, *26*, 5–16. [[CrossRef](#)]
49. Shannon, R.D. Revised effective ionic radii and systematic studies of interatomic distances in halides and chalcogenides. *Acta Crystallograph. Sect. A* **1976**, *32*, 751–767.
50. Gervasini, A. *Temperature Programmed Reduction/Oxidation (TPO/TPR) Methods in Calorimetry and Thermal Methods in Catalysis*; Auroux, A., Ed.; Springer: New York, NY, USA, 2013; pp. 175–196.
51. Kubiak, L.; Castoldi, L.; Lietti, L.; Andonova, S.; Olsson, L. Mechanistic Investigation of the Reduction of NO_x over Pt- and Rh-Based LNT Catalysts. *Catalysts* **2016**, *6*, 46. [[CrossRef](#)]
52. Andonova, S.; Marchionni, V.; Borelli, M.; Nedyalkova, R.; Lietti, L.; Olsson, L. Mechanistic investigations of the promoting role of Rh on the NSR performance of NO_x storage BaO-based catalysts. *Appl. Catal. B Environ.* **2013**, *132–133*, 266–281. [[CrossRef](#)]
53. Castoldi, L.; Matarrese, R.; Daturi, M.; Llorca, J.; Lietti, L. Al₂O₃-supported Pt/Rh catalysts for NO_x removal under lean conditions. *Appl. Catal. A Gen.* **2019**, *581*, 43–57. [[CrossRef](#)]
54. Raj, R.; Harold, M.P.; Balakotaiah, V. Steady-state and dynamic hysteresis effects during lean co-oxidation of CO and C₃H₆ over Pt/Al₂O₃ monolithic catalyst. *Chem. Eng. J.* **2015**, *281*, 322–333. [[CrossRef](#)]
55. Arvajova, A.B.; Březina, J.; Pečinka, R.; Kočí, P. Modeling of two-step CO oxidation light-off on Pt/γ-Al₂O₃ in the presence of C₃H₆ and NO_x. *Appl. Catal. B Environ.* **2018**, *233*, 167–174. [[CrossRef](#)]
56. Hazlett, M.J.; Moses-Debusk, M.; Parks, J.E., II; Allard, L.F.; Epling, W.S. Kinetic and mechanistic study of bimetallic Pt-Pd/Al₂O₃ catalysts for CO and C₃H₆ oxidation. *Appl. Catal. B Environ.* **2017**, *202*, 404–417. [[CrossRef](#)]
57. Ferre, G.; Aouine, M.; Bosselet, F.; Burel, L.; Aires, F.C.S.; Geantet, C.; Ntais, S.; Maurer, F.; Casapu, M.; Grunwaldt, J.-D. Exploiting the dynamic properties of Pt on ceria for low-temperature CO oxidation. *Catal. Sci. Technol.* **2020**, *10*, 3904–3917. [[CrossRef](#)]
58. Lang, W.; Laing, P.; Cheng, Y.; Hubbard, C.; Harold, M.P. Co-oxidation of CO and propylene on Pd/CeO₂-ZrO₂ and Pd/Al₂O₃ monolith catalysts: A light-off, kinetics, and mechanistic study. *Appl. Catal. B Environ.* **2017**, *218*, 430–442. [[CrossRef](#)]